RSC Advances

PAPER

View Article Online
View Journal | View Issue

Cite this: *RSC Adv.*, 2023, **13**, 14384

Remarkable synergy between sawdust biochar and attapulgite/diatomite after co-ball milling to adsorb methylene blue†

Fei Jiang,[a] Feiyue Li, ‡*[a] Andrew R. Zimmerman,[b] Zhongpu Yu,[a] Licheng Ji,[a] Chengcheng Wei,[a] Xueyang Zhang[d] and Bin Gao [c]

Biochar has been recognized as a promising sustainable adsorbent for removing pollutants from wastewater. In this study, two natural minerals, attapulgite (ATP) and diatomite (DE) were co-ball milled with sawdust biochar (pyrolyzed at 600 °C for 2 h) at ratios of 10–40% (w/w) and examined the ability of methylene blue (MB) to be removed from aqueous solutions by them. All the mineral-biochar composites sorbed more MB than both ball milled biochar (MBC) and ball milled mineral alone, indicating there was a positive synergy in co-ball milling biochar with these minerals. The 10% (w/w) composites of ATP:BC (MABC10%) and DE:BC (MDBC10%) had the greatest MB maximum adsorption capacities (modeled by Langmuir isotherm modeling) and were 2.7 and 2.3 times that of MBC, respectively. The adsorption capacities of MABC10% and MDBA10% were 183.0 mg g^{-1} and 155.0 mg g^{-1} at adsorption equilibrium, respectively. These improvements can be owing to the greater content of oxygen-containing functional groups and higher cation exchange capacity of the MABC10% and MDBC10% composites. In addition, the characterization results also reveal that pore filling, π–π stacking interactions, hydrogen bonding of hydrophilic functional groups, and electrostatic adsorption of oxygen-containing functional groups also contribute prominently to the adsorption of MB. This, along with the greater MB adsorption at higher pH and ionic strengths, suggests the roles in MB adsorption was an electrostatic interaction and an ion exchange mechanism. These results demonstrate that mineral-biochar composites prepared by co-ball milling treatment were promising sorbents of ionic contaminants for environmental applications.

Received 20th February 2023
Accepted 7th April 2023

DOI: 10.1039/d3ra01123b

rsc.li/rsc-advances

1 Introduction

Every year, about 7×10^5 t of dyes were produced for printing and dyeing industries. Inevitably, some portion of the dyes (less than 15%) are discharged directly or indirectly into aquatic environment, endangering human and ecological health. Hence, technologies were required to remove dyes from waste and contaminated waters. The methods for treating dye wastewater include photocatalysis, ozone oxidation and adsorption. However, the adsorption method was widely used because of its simplicity, economy and high efficiency. Hence, many scientists were working on developing cost-effective adsorbents. Common adsorbents mainly include clay, activated carbon, graphene, *etc.* However, production of these materials is often costly and associated with high energy consumption and environmental damage.[1]

In recent years, biochar (BC) has received extensive attention as a novel adsorbent for the removal of pollutants from water, soil, and air. BC was a porous solid material formed by pyrolysis of solid biomass waste in an anaerobic environment. It has advantageous properties including high aromaticity and abundant oxygen-containing functional groups, specific surface area, and favourable cation exchange capacity, all of which were conducive to adsorption of pollutants. In that it can be generated from waste or recycled materials and was carbon-neutral or negative, BC was considered a promising adsorbent for various environmental applications.

Numerous studies have suggested that the adsorption efficiency of BC may be improved by chemical or physical modification or by compounding with other materials.[2–4] Recently, many studies have shown that ball milling technology is considered as a promising method for BC modification.[5,6] The non-equilibrium mechanical force generated by collision with

[a]*College of Resources and Environment Science, Anhui Science and Technology University, Fengyang, 233100, China. E-mail: lify@ahstu.edu.cn*

[b]*Department of Geological Sciences, University of Florida, Gainesville 32611, FL, USA*

[c]*Department of Agricultural and Biological Engineering, University of Florida, Gainesville 32611, FL, USA*

[d]*School of Environmental Engineering, Jiangsu Key Laboratory of Industrial Pollution Control and Resource Reuse, Xuzhou University of Technology, Xuzhou 221018, PR China*

† Electronic supplementary information (ESI) available. See DOI: https://doi.org/10.1039/d3ra01123b

‡ Equal contribution to the paper.

and extrusion between grinding beads reduces particle sizes to nano-scales.

Ball milling of BC has been shown to increase the type and number of surface functional groups, specific surface area and pore volume of BC, thus increasing its adsorption capacity for pollutants.[7–9] For example, ball milling of bamboo and hickory chip biochar produced a range of functional groups which greatly enhanced the adsorption of sulfamethoxazole and sulfapyridine antibiotics *via* hydrogen bonding, and hydrophobic, π–π, and electrostatic interactions.[7,10] In addition, ball-milling technology has advantages over chemical modification techniques in terms of its low consumption, simple method and adaptability to large-scale production, that make it suitable for producing environmentally friendly-engineered BC sorbents.[5]

Co-ball milling of biochar with other materials has also proven promising. For example, ball milling CuO or MgO particles with BC produced nanocomposites that can remove various contaminants from aqueous solution.[11,12] In addition, co-ball milled biochar and iron oxide nanocomposites have exhibited high sorption ability as well as magnetic property.[13,14] In regards to co-ball milling with clays, Yang *et al.*[15] reported excellent methylene blue (MB) removal (72.1 mg g^{-1}) by co-ball milled biochar and montmorillonite. Li *et al.*[16] reported that a ball-milled composite of 20% hickory biochar (600 °C) and 80% expanded vermiculite removed As(v) from aqueous solution to a much greater extent than ball-milled biochar or ball-milled expanded vermiculite. The reason for this was thought to be the large pore volume and surface area, significant changes in crystallinity, activation of cations, and increase of functional groups in the nanocomposites. Clearly, the nature of mineral-biochar composite depends on many factors including the types of biochar and additives.

Attapulgite (ATP) and diatomite (DE) are two natural minerals (commonly referred to as minerals although diatomite was not technically a mineral) that have been used to adsorb pollutants owing to their developed porosity, high specific surface area, abundant active sites, *etc.*[17] Besides, they are abundant, highly stabile, and environmentally friendly.[18] Studies have shown that the surface properties of biochar materials were enhanced by doping minerals and have obvious effects, which is owing to the synergistic effect between oxygen-containing surface functional groups and layered mesoporous structure, therefore, it was helpful for the biochar-based clay composites to be chemisorbed by MB through cation exchange.[19] Given that co-ball milling of biochar with minerals/metal oxides has produced many excellent composite adsorbents, it was likely that this technique may be useful to combine the strong sorption ability of ATP and DE with that of biochar, creating synergy to adsorb MB in aqueous solution.

In addition, there are relatively few studies on the preparation of adsorbents from ball-milled biochar and attapulgite/diatomite. Here, the attapulgite and diatomite-biochar composites (ATP–BC and DE–BC, respectively) of different mineral/biochar weight ratios were prepared by co-ball milling. The composites were characterized and tested to adsorb MB, a common dye that is widely used as a model compound to study dye adsorption. The main objectives of this study are as follows: (1) the physical and chemical properties of the mineral-biochar composite are characterized, (2) the weight ratio of the composites to adsorb MB is optimized, and (3) the adsorption mechanism of the mineral-biochar composite was understood through a series of Batch MB adsorption study.

2 Materials and methods

2.1 Materials

ATP and DE were purchased from Guangxi Donglong Chemical Company (chemical grade), China. The main component of ATP was magnesium aluminosilicate but contains a small amount of Ca^{2+}. The molecular formula was SiO_2 but it also contains a small amount of impurities. MB was purchased from Tianjin Guangfu Institute of Fine Chemicals (analytical grade), and its molecular formula was $C_{16}H_{18}ClN_3S\cdot 3H_2O$.

2.2 Adsorbent preparation

Coarse sawdust was collected from wood processing plants in BengBu, PRC, passed through a 1 mm sieve to remove the coarse slag. To prepare the biochar, sieved sawdust was placed in quartz boats and placed into a horizontal tube furnace (OTF-1200X, Hefei Kejing). The oven was an oxygen-free environment created by N_2 flowing at 2 mL min^{-1}, the heating rate was 10 °C min^{-1}, the peak temperature was 600 °C, which was held for 2 h.[20]

To produce the mineral-biochar composites, ATP or DE was added to BC at mass ratios of 10%, 20%, 30% and 40%. Put the mixture into a vertical planetary ball mill (XQM-2, Tencan™) and was run with a rotation speed 400 rpm min^{-1}, in forward and reverse directions, each for 60 min with a 10 min rest interval, repeated 3 times.[21] The mineral-biochar (co-ball-milled) composites were designated with letters indicating mineral, BC and weight ratio. For example, MABC10% is that the ball-milled composite of 10% attapulgite and 90% BC (w/w). For comparison, minerals and biochar were separately ball-milled and then physically mixed and were designated with CK (*e.g.* MABC10%-CK). Control treatments also included BC, ATP, and DE ball milled separately, and were designated MBC, MATP, and MDE, respectively.

2.3 Sorbent characterization

Determination of elemental composition (C, H and N) of selected adsorbents (MBC, MABC10% and MDBC10%) using an Elemental Analyzer (Vario ELIII, Elementar, Germany). The surface morphologies and energy-dispersive spectra (EDS) of these materials were observed by scanning electron microscopy (EVO® 18, Carl Zeiss, UK). The Brunauer–Emmett–Teller (BET) specific surface area and pore volume of those materials were determined *via* dinitrogen sorptometry (Autosorb iQ, Quantachrome Instruments, USA). Thermal stability was measured on a thermogravimeter (TG-DTG, STA-449F5, Netzsch, Germany) over a 35 °C to 900 °C range at a heating rate of 20 °C min^{-1}. Crystal phases of select sorbents were determined by X-ray diffraction (XD-3, Beijing Puxi, PRC), with the scanning range (2θ) of 10–90° at scan speed $2°\cdot min^{-1}$. Raman

spectroscopy (XploRA Plus, Horiba, Germany) was used to detect the number of functional groups and the degree of graphitization of the adsorbents, using a range of 500–2000 cm^{-1}. Functional group distribution was recorded using a Fourier transform infrared spectrometer (FTIR-850, Tianjin Gangdong Technology, PRC) with the range of 4000–500 cm^{-1}. Finally, Cation exchange capacity (CEC) was analyzed spectrophotometrically by hexaammine cobalt trichloride solution.[22]

2.4 MB adsorption

To determine the optimal weight ratio of ATP–BC and DE–BC for MB adsorption, the adsorption capacities of both ball-milled mineral composites (with different addition ratios from 0 to 40%) and control samples (biochar or mineral alone and their ball milled products) were tested. Briefly, 0.05 g of each sorbent and 40 mL of 200 mg L^{-1} MB solution was put into 50 mL Teflon tubes, and oscillated at 160 rpm min^{-1} for 24 h in a constant temperature (25 ± 1 °C) shaking incubator. Each treatment was carried out in triplicate. The samples were then filtered with a 0.45 μm (PES) filter, and MB in the filtrate was determined *via* spectrophotometer (722G, Shanghai Jinke) at the absorbance wavelength of 668 nm.

For adsorption isotherm experiments, 50 mg of MABC10% and MDBC10% were mixed with 40 mL MB solutions in concentrations ranging from 150 mg L^{-1} to 400 mg L^{-1}. For adsorption kinetic experiments 50 mg so bent was added to 200 mg L^{-1} MB solutions and sampling time points were 5 min to 1440 min, Other experimental procedures were the same as the described above.

The effects of initial pH (adjust to 2 to 10 with 0.1 mol L^{-1} HCl and/or NaOH) and ionic strength (use a $NaNO_3$ solution with a concentration of 0 to 0.1 mol L^{-1}) on MB adsorption by select sorbents were investigated using conditions the same as those of the optimal weight ratio testing.

2.5 Data analysis

Adsorption was calculated as the amount of MB in the initial test solution, less the amount in the filtrates. Experimental data were analyzed using adsorption capacity equations, removal rate equations, Freundlich and Langmuir adsorption isotherm model, and pseudo-first-order and pseudo-second-order adsorption kinetic models, which were detailed in the ESI† as well as referenced in a previous study.[23] The data for the adsorption performance, kinetics and adsorption isotherms of the selected materials were presented in the ESI.†

3 Results and discussion

3.1 Effects of the mineral addition ratio of composites on MB adsorption

The MB adsorption capacity of the original materials (biochar or mineral) was low: 0.7 mg g^{-1} for BC, 76.0 mg g^{-1} for ATP, and 0.61 mg g^{-1} for DE, respectively (Fig. 1). After they were ball-milled, BC and DE increased the adsorption of MB by 101-fold and 35.5-fold, but decreased by 2.2-fold for ATP, indicating that ball milling could be an effective method to improve the adsorption capacity of some materials, but its effect depends on material type. Combining ball milled biochar with ball milled minerals (CK samples) further increased MB adsorption. However, the mineral-biochar composites produced by co-ball milling biochar with minerals increased the MB adsorption capacity even more, indicating there was a positive synergy in terms of creating MB adsorption capacity *via* co-ball milling.[14,24] Specifically, MB adsorption by MABC10% was 46.1% greater than that of MABC10% CK (the 10% mixture of attapulgite and biochar separately ball-milled).

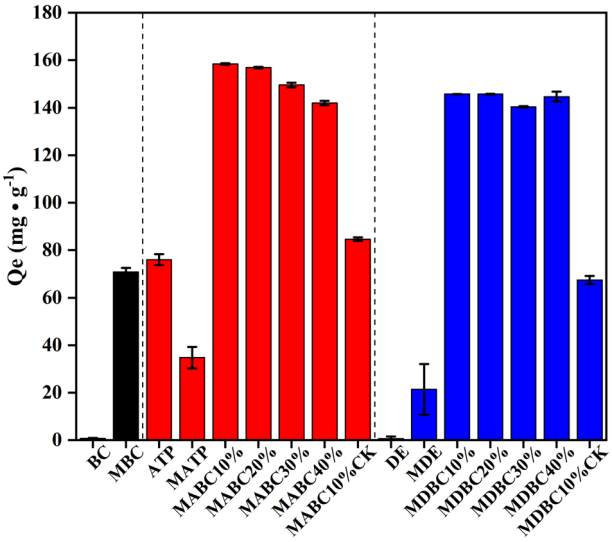

Fig. 1 MB adsorption capacity of sawdust biochar (BC), attapulgite (ATP), diatomite (DE), their ball-milled forms (MBC, MATP, and MDE) and their co-ball-milled forms (MABC and MDBC) produced at different weight ratios (%biochar/mineral) and using 200 mg L^{-1} MB solutions. Sorbents composed of separately ball-milled biochar and mineral mixtures are designated as CK. Bars are means of triplicate analyses and uncertainty bars are standard deviation.

For each given weight ratio, co-ball milled attapulgite with biochar generally sorbed more MB than co-ball milled diatomite with biochar (by 8.71%, on average). This was because when biochar and mineral co-grinding materials adsorb MB, part of the adsorption in the cooperative adsorption was the adsorption capacity of the raw materials themselves. It can be seen from Table S1† that the adsorption effect of attapulgite on MB before and after ball milling was higher than that of diatomite. Therefore, attapulgite co-milled with biochar generally adsorbed more MB than diatomaceous earth co-milled with biochar. In addition, the materials with the highest adsorption capacity for MB were MABC10% (158.32 mg g^{-1}) and MDBC10% (145.64 mg g^{-1}). For example, MABC10% sorbed 0.94%, 5.52%, and 10.21% more than MABC20%, MABC30% and MABC40%, respectively. Since 10% mineral was the optimal weight ratio, MABC10% and MDBC10% were selected for subsequent individual characterization tests and extensive batch adsorption experiments.

3.2 Sorbent characterization

Compared with that of MBC, the C contents of MABC10% and MDBC10% were 12.7% and 12.5% lower, and the N contents

were 23.8% and 33.3% lower. This was surely due to the dilution effect of 10% mineral addition (Table S2†). In contrast, the O contents of MABC10% and MDBC10% were 32.7% and 9.59% greater than that of MBC, respectively. This implies that the attapulgite was particularly oxygen-rich. All of which led to the H/C and O/C increasing by 15.7% and 52.1% for MABC10%, and 4.64% and 25.6% for MDBC10% compared with MBC, indicating MABC10% and MDBC10% enriched in oxygen-containing functional groups that may facilitate their adsorption of pollutants. In addition, the CEC of MABC10% and MDBC10% increased by 6.7 and 1.3 times compared with that of MBC. Ball milling may lead to exposure of the patterned structure of biochar, thereby increasing CEC through strong cation–π interactions.[25,26] This is likely due to the high CEC of ATP and DE minerals.[1,27]

Compared with the specific surface area and pore volume of MBC, MABC10% decreased by 21.8% and 18.8%, and MDBC10% decreased by 17.5% and 16.1%, respectively (Table S1†). This may be due to the mechanical force in the ball milling process, the ATP and DE particles were embedded in the pores or inter layers of the BC, thereby plugging the pores resulting in a reduced specific surface area and a reduced pore volume.[8,28,29] Studies have also shown that the micropores of carbon materials are blocked and the specific surface area is reduced, which may be the reason for the functional groups on the surface of biochar.[30] Moreover, the average pore size of MABC10% and MDBC10% was larger than that of MBC (Table S1†), which may be due to the destruction of the biochar pore structure during the ball milling process, and mineral particles are squeezed and embedded in the destroyed pore.[28]

The SEM-EDS images of MBC, MABC10% and MDBC10% showed that ATP and DE became embedded in the pores of the BC during ball milling.[8,31,32] This likely led to the decrease in SA and pore diameters observed in BET-analyses (Table S2†). Moreover, the distribution of Ca in MABC10% and Si in MDBC10% (Fig. 2b and c), respectively, suggests a relatively homogenous coverage of minerals on the biochar surfaces, which may be beneficial for increasing contaminant adsorption.

TGA-DTG analysis of MBC, MABC10% and MDBC10% are shown in Fig. 3a. Below 300 °C, the mass loss of MBC, MABC10% and MDBC10% were very small due to the consumption of volatiles on the material surface, and the moisture of external physical adsorption in the materials loss. With the temperature increasing, the mass loss of those materials enlarged, caused by the loss of bound water within the structure of the material containing minerals and the decomposition of organic matter. At 500–900 °C, the mass loss of the material were much smaller, which may be due to the residual inorganic salt ash residue after the combustion of the three materials in the air atmosphere. Compared with MBC, the TGA-DTG curve of MABC10% pulled back greatly when the temperature over about 400 °C, indicating that ATP addition for ball milling improved its oxidation-resistance stability. Conversely, for MDBC10%, its weight loss was much higher than that of MBC (Fig. 3a), indicating that DE addition for ball milling enlarged its decomposition. The MABC10% was enriched in Ca based on SEM-EDS analysis (Fig. 2), and it was beneficial for improving its oxidation-resistance stability.[33,34]

The XRD patterns of MBC, MABC10% and MDBC10% all exhibited two broad XRD diffractions peaks ($2\theta = 24°$, $2\theta = 43°$) (Fig. 3b). Both are plans of graphite, (002) and (100), respectively, and the former was traditionally used to estimate the degree of carbon graphitization.[35–37] For MABC10%, there were three characteristic peaks (2θ = 30.6°, 40.8° and 50.7°) that correspond to attapulgite (JCPDS No. 21-0958) and MDBC10% showed peaks of amorphous opal-A at $2\theta = 21.6°$.[35] In addition, $2\theta = 14.03°$ can be attributed to the (200) crystal phase plane of MBC, $2\theta = 16.12°$ can be attributed to the (130) crystal phase plane of diatomite, and $2\theta = 20.67°$ can be attributed to the attapulgite (400) crystal plane.[38] These further confirm that the mineral-biochar composites had ATP or DE on their surfaces.[39–41] The results correspond to the SEM-EDS images (Fig. 2), showing that ATP or DE mineral were embedded or attached to the BC surface, forming the ABC10% or DBC10% composites.

The Raman spectra of MBC, MABC10% and MDBC10% are shown in Fig. 3c. Two typical peaks at about 1340 cm^{-1} and about 1580 cm^{-1} associated with the D and G bands were clearly visible. The D band was used to indicate the impurities in the carbon, the structural integrity of C is represented by the G peak, and the I_D/I_G value (D peak/G peak) was used to indicate the degree of graphitization of the carbon and functional groups in the carbon material abundance.[40] I_D/I_G values less than 1 and greater than 1 were used to indicate the degree of graphitization and the number of functional groups, respectively.[41] The I_D/I_G ratios of the three adsorbents were in the order MBC > MABC10% > MDBC10% > 1. Therefore, all three

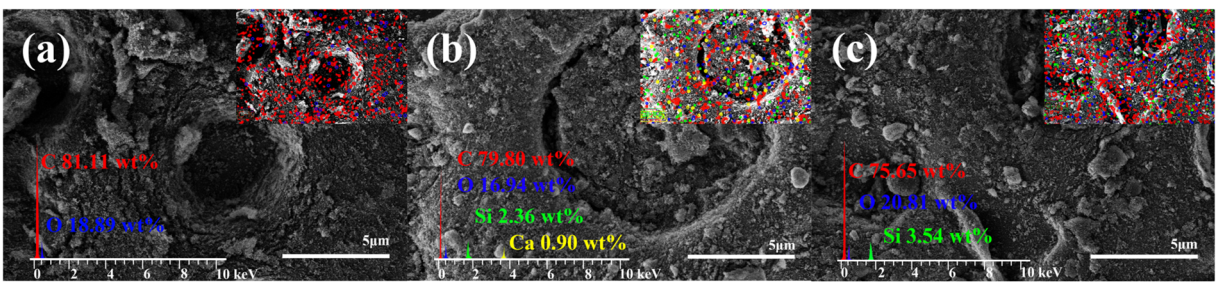

Fig. 2 SEM images of selected ball-milled adsorbents (a) MBC, (b) MABC10% and (c) MDBC10%. The upper right corner of the SEM image shows the EDS image corresponding to the adsorbent, and the lower left corner shows the proportion of elements scanned by EDS.

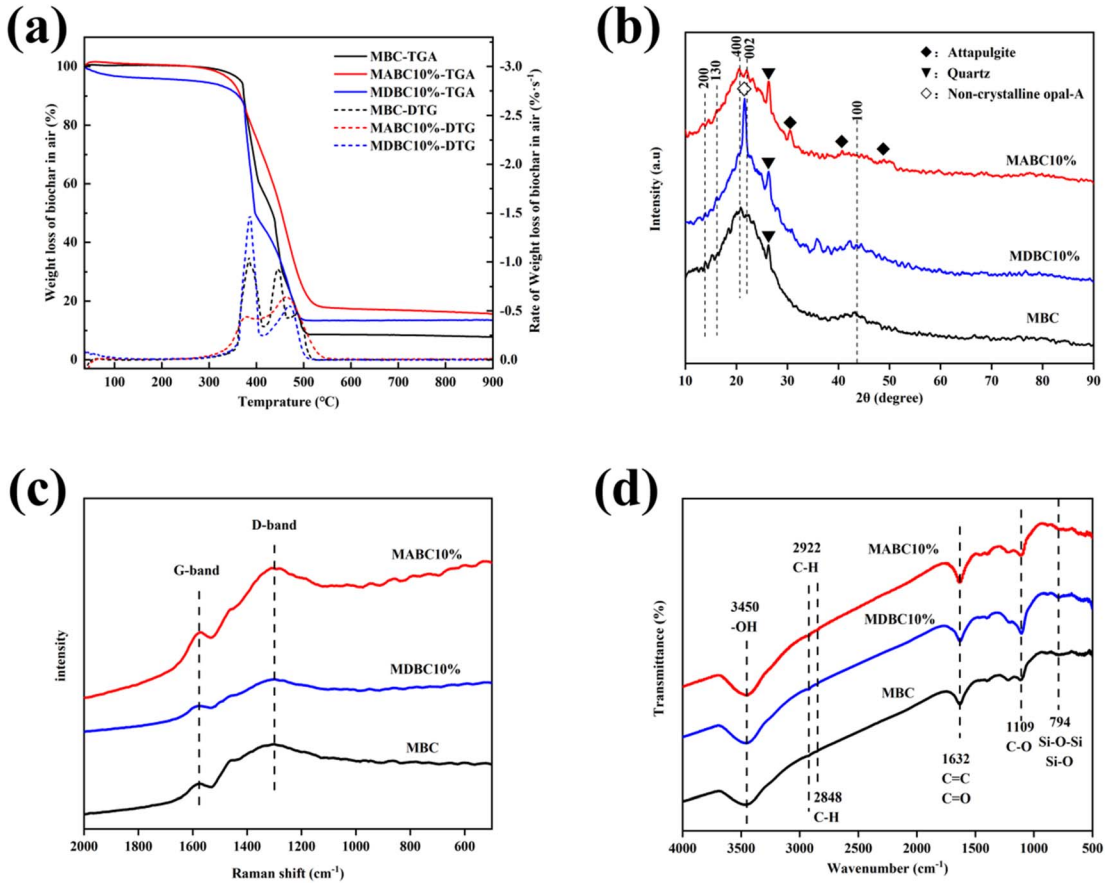

Fig. 3 Characterization of selected ball milled sorbents MBC, MABC10% and MDBC10% by TGA (a) and XRD (b), Raman (c) and FTIR (d) spectroscopy.

adsorbents were rich in functional groups.[39] Calculated from the D peak and G peak integration of these three materials, the I_D/I_G value of MBC was much higher than that of MABC10% and MDBC10%, which may be that more minerals were introduced by ball milling to destroy the structure of C element.[42] The I_D/I_G ratios of MABC10% and MDBC10% were closer to 1 with few change, which may be due to that the addition of ATP and DE reduced the grain size of the C unit and promoted the amorphous structure and lattice defects of C.[37,43]

FTIR spectra of MBC, MABC10% and MDBC10% are shown in Fig. 3d. A peak of the –OH stretching vibration around 3450 cm^{-1} was observed. The bands located at 2922 cm^{-1} and 2848 cm^{-1} correspond to the C–H asymmetric and symmetric stretching vibration. The absorption band around 1632 cm^{-1} is ascribed to the skeletal vibration of C=C in the aromatic structure or the C=O stretching vibration that can be assigned to –COOH in aromatic compounds, which may provide adsorption sites for the attachment of organic pollutants.[1] The peak at 1109 cm^{-1} is likely to be C–O, while the peak at 794 cm^{-1} may be the impurity SiO_2 in quartz or amorphous opal. Active sites for adsorption of organic pollutants were provided by the presence of siloxane O–Si bonds through n–π interactions.[1,7,36] Studies have indicate that –OH and –COOH were believed to play catalytic roles in the adsorption mechanism of MB on biochar materials.[44] In addition, many oxygen-containing functional groups of MABC10% and MDBC10% make them hydrophilic and good dispersibility, which is beneficial to their adsorption of cationic MB in aqueous solution.[30]

3.3 MB adsorption isotherms

The MB adsorption isotherms showed that, at all initial MB concentrations, adsorption capacity followed the order: MABC10% > MDBC10% ≫ MBC (Fig. 4a). For each of the sorbents, the amount of MB adsorbed increased quickly with increasing initial MB concentrations, reaching maximum adsorption capacities at initial MB concentrations of about 25 mg L^{-1} equilibrium concentration.

In order to further study the adsorption performance and mechanism of these adsorbents for MB, the adsorption isotherm model (Freundlich and Langmuir) was used in this study to conduct simulation experiments (Fig. 4a and Table S3†). The higher R^2 values simulated for these materials indicate that the Langmuir model provides a better fit to the adsorption isotherm data. This finding was similar to reported studies on MB adsorption to modified bamboo charcoal[45,46] and as adsorption to a biochar-vermiculite nanocomposite.[23] This

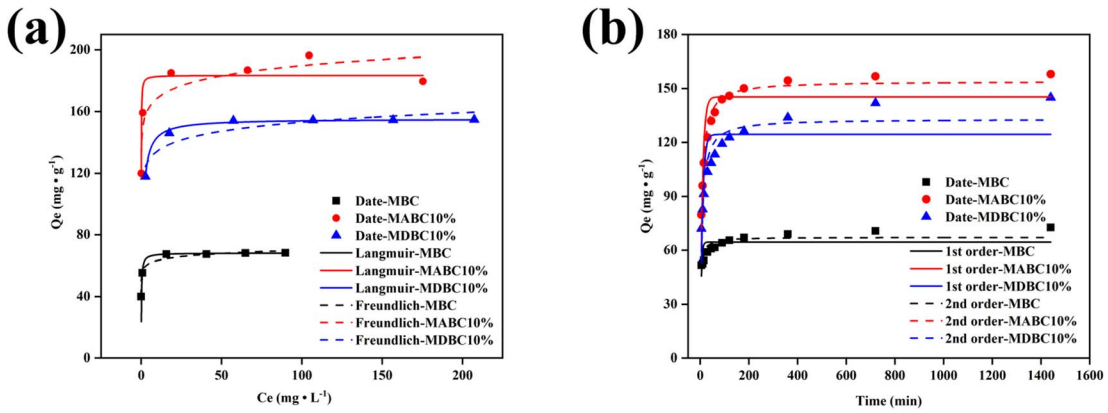

Fig. 4 Adsorption isotherms (a) and adsorption kinetics (b) of MB adsorbed by MBC, MABC10% and MDBC10%.

suggests that MB adsorption may be monolayer adsorption and relatively homogeneous across the surface active sites.

The adsorption capacity (Qm) of MABC10% and MDBC10% simulated by Langmuir was 185 and 155 mg g^{-1}, 2.7 and 2.3 times that of MBC, respectively. Given that the SA of MBC was higher than that of MABC10% and MDBC10% and that of MDBC10% was higher than that of MABC10% (Table S2†), the main adsorption mechanism of MB was considered unlikely to be physical adsorption. CEC of the sorbents also poorly corresponded to MB adsorption capacity (Table S2†). Therefore, the increase in oxygenated functional groups and the synergy of mesoporous layered structures caused by the addition of minerals (attapulgite/diatomaceous) co-ball grinding are perhaps considered the most important factors.[30]

Compared with many other sorbents, MABC10% and MDBC10% had shorter equilibration times and greater MB maximum adsorption capacities (Table 1). As shown in Table 1, the adsorption capacity of the biochar material obtained by carbonization from 200 °C to 600 °C for MB was much smaller than that of MABC10% and MDBC10%. Even at the same temperature of 600 °C, the adsorption performance and adsorption capacity of the biochar-based mineral composites in this study were higher than those of the studies listed in the Table 1 (MABC10%: 2.54–6.38 times; MDBC10%: 2.15–5.40 times).

3.4 Kinetics of MB adsorption

The adsorption kinetics curves of the three materials MB showed that the adsorption was mainly occurred in the first 180 min and the adsorption equilibrium time did not exceed 240 min (Fig. 4b). The adsorption kinetics of these materials for MB was simulated by a pseudo-second-order model (Fig. 4b and Table S3†). This suggests that in the process of MB adsorption, the adsorption mechanism may be controlled by other multi-mechanism factors such as adsorption sites and interactions. The study shows that van der Waals forces, π–π and electrostatic interactions were considered to be the main adsorption

Table 1 Comparison of MB adsorption by different adsorbents

Adsorbents	Preparation temperature (°C)	Q_m (mg g^{-1})	Reference
Wheat straw biochar	200	46.6	52
Municipal sewage sludge and tea waste biochar	300	12.6	(Fan *et al.*, 2016)[53]
Hickory biochar	350	16.3	54
Anaerobic digestion residue biochar	400	9.5	(Sun *et al.*, 2013)[55]
Palm bark biochar	400	2.7	55
Eucalyptus biochar	400	2.1	55
Rabbit feces biochar	500	104.0	56
Pig manure biochar	500	53.7	56
CMC	600	58.6	(Yang *et al.*, 2020)[19]
Montmorillonite	600	13.3	(Yang *et al.*, 2020)[19]
Biochar-based montmorillonite	600	72.1	(Yang *et al.*, 2020)[19]
Calcite	600	9.3	(Yang *et al.*, 2020)[19]
Biochar-based calcite	600	32.1	(Yang *et al.*, 2020)[19]
Quartz	600	9.9	(Yang *et al.*, 2020)[19]
Biochar-based quartz	600	28.7	(Yang *et al.*, 2020)[19]
MBC	600	68.2	This study
MABC10%	600	183	This study
MDBC10%	600	155	This study

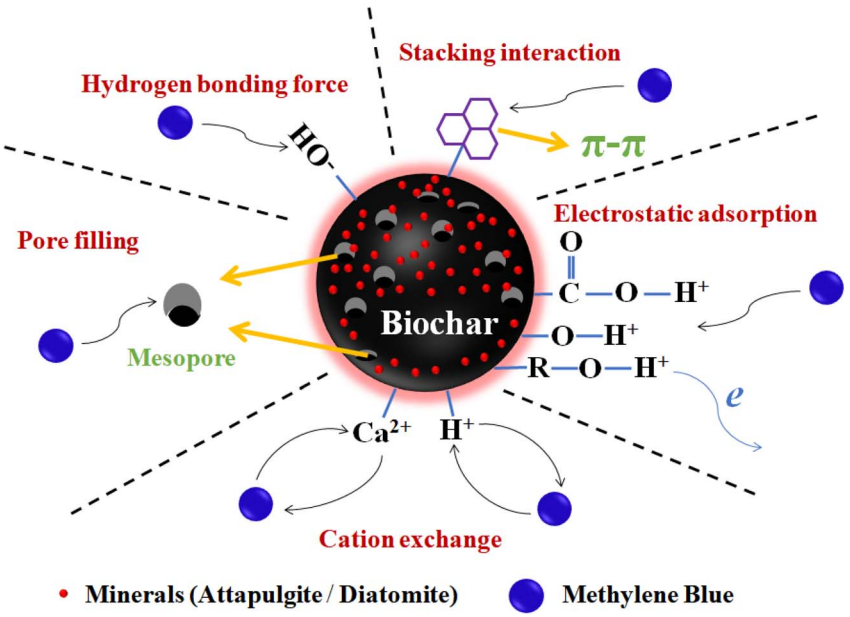

Fig. 5 Possible pathways and mechanisms of MB removal by biochar-based materials (10% MABC/10% MDBC).

mechanisms of MB on biochar. MBs were bound to functional groups and aromatic structures of biochar through ion exchange and π–π interactions, respectively.[25,26]

According to the above analysis, the main mechanism of removing MB by MABC10% and MDBC10% can be divided into the following parts (Fig. 5): (1) the high porosity (specific surface area and total pore volume) of the biochar surface adsorbs MB through pore filling; (2) the hydrogen bonding of hydrophilic functional groups (mainly –OH and –COOH) on the surface of biochar and the electrostatic adsorption of oxygen-containing functional groups adsorbed MB; (3) adsorption of MB through π–π stacking interaction on the surface of biochar; (4) the biochar material treated with mineral ball milling has a cation exchange effect to adsorb cationic dye MB.

3.5 pH and ionic strength effects

When solution pH was increased from 2 to 10, MB adsorption increased from 50.2 mg g^{-1} to 93.4 mg g^{-1} (86.06%) for MBC, from 109.0 mg g^{-1} to 153.5 mg g^{-1} (40.83%) for MABC10%, and from 125.1 mg g^{-1} to 159.3 mg g^{-1} (27.34%) for MDBC10%, respectively (Fig. 6a). This is likely due to the effects of solution pH on the number of charges on the surface and the electrolysis of functional groups. Under acidic conditions, active sorption sites would be protonated, resulting in electrostatic repulsion of cationic MB. The same binding site may also be competed with MB^+ by excess H^+.[47] With increasing pH, MB adsorption capacity increased as active sites became deprotonated and cation competition decreased. The effect of the initial pH of the solution on the adsorption of MB by the adsorbent indicated that the electrostatic force interaction was considered as one of the important factors for the adsorption of MB dyes by biochar-based mineral composites. With no added minerals, the cation exchange capacity of MBC sorbent is lower than that of MABC10% and MDBC10%, so it was more easily affected by ions in solution when the pH was too high or too low. The reason why MDBC10% adsorbed more MB than MABC10% at

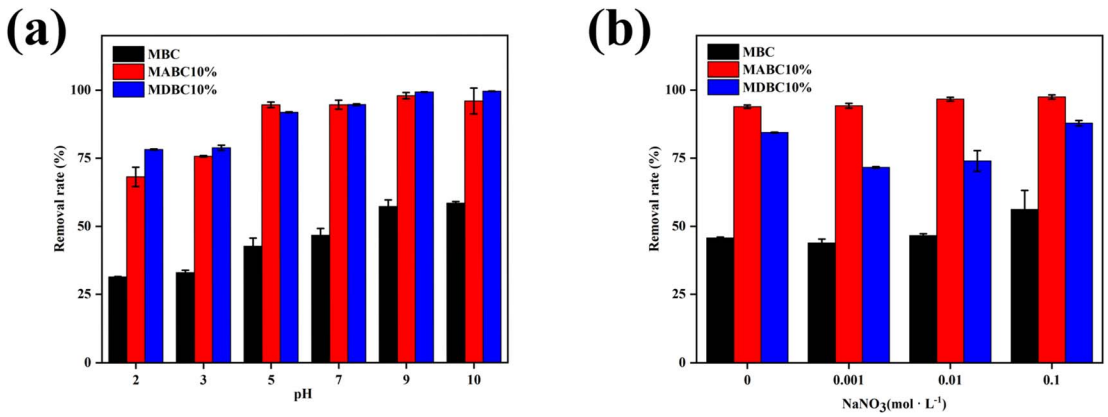

Fig. 6 Effects of initial pH (a) and ionic strength (b) on MB adsorption onto selected ball milled sorbents.

low pH and high pH was attributed to the repulsion between MABC10% metal ions (Ca^{2+}, Mg^{2+}, *etc.*) and H^+ in a low pH environment. At high pH, MDBC10% carried more negative charges, which was more favorable for the adsorption and removal of cationic dye MB.

Ionic strength ($NaNO_3$, 0 to 0.1 mol L^{-1}) was found to have only a small effect on MB removal which increased by only 22.56%, 4.10%, and 3.80% for MBC, MABC10% and MDBC10% (Fig. 6b). In previous studies, the ionic strength of the solution has been shown to be one of the factors that has an important influence on the results of adsorption experiments.[57,58] The increase in ionic strength may reduce the solubility of MB in aqueous solution, thereby helping more MB molecules to diffuse to the surface of the biochar composite, a phenomenon known as the salting-out effect.[48,49] Another reason may be that a non-electrostatic force occurs during the adsorption process between MB and biochar composites, and a slight increase in ions leads to an increase in the non-electrostatic force, which is due to the occurrence of electrostatic repulsion.[50] It may be that increasing ionic strength had only minimal effect of MB adsorption to the biochar-mineral composites because with the help of non-electrostatic forces, a dispersive interaction occurred between the MB molecules and the surface or basal-294 plane of the biochar composite, causing in an increase in the adsorption capacity.[51]

4 Conclusions

In this study, the novel mineral biochar composite prepared from ball mill sawdust biochar with minerals (attapulgite and diatomaceous earth) can remove MB more effectively than ball mill sawdust biochar (MBC) in aqueous solution. Among them, the mineral biochar composites made of 10% attapulgite and diatomaceous earth had the highest MB removal rate, and the adsorption capacity was 183.0 mg g^{-1} and 155.0 mg g^{-1} during equilibrium time, respectively. The characterization results show that in addition to the hydrogen bonding of hydrophilic functional groups and electrostatic adsorption of oxygen-containing functional groups, cation exchange also makes outstanding contributions to the adsorption of MB. At the same time, pore filling, π–π stacking interaction also helps remove MB. Higher pH to MB removal rate indicates the importance of electrostatic interactions and CEC in MB adsorption. The presence of coexisting ions does not significantly affect the removal of MABC10% and MDBC10%. Therefore, the mineral-biochar composite developed here is a promising low-cost and environmentally friendly alternative adsorbent. In order to optimize the preparation process of mineral-biochar composites to remove environmental pollutants such as MB in water, further research was needed.

Data availability

The datasets used and/or analyzed during the current study are available from the corresponding author on reasonable request.

Author contributions

Conceptualization, data curation, visualization, writing-original draft, Fei Jiang; resources, writing – review & editing, funding acquisition, Feiyue Li; writing – review & editing, data curation, Andrew R. Zimmerman; writing– review & editing, methodology, Zhongpu Yu; data curation, Licheng Ji; methodology, data curation, validation, Chencheng Wei; formal analysis, project administration, investigation, Xueyang Zhang; funding acquisition, project administration, writing– review & editing, Bin Gao.

Conflicts of interest

The authors declare that they have no known competing financial interests or personal relationships that could have appeared to influence the work reported in this paper.

Acknowledgements

The authors would like to acknowledge the support of Anhui Province University Top Talent Funding Project (gxbjZD2021069); The Anhui Science and Technology Major Project (201903a06020023, 201903a06020001); Natural Science Research Project of Colleges and Universities in Anhui Province (KJ2020A0049); Commissioned R&D Project (ZHEP2021001, BOFA202007); Anhui Provincial Graduate Education Quality Engineering – Graduate Academic Innovation Project (2022xscx140).

Notes and references

1 F. Meng, M. Song, Y. Chen, Y. Wei, B. Song and Q. Cao, *Environ. Sci. Pollut. Res. Int.*, 2021, **28**, 11106–11118.
2 Y. Qin, X. Zhu, Q. Su, A. Anumah, B. Gao, W. Lyu, X. Zhou, Y. Xing and B. Wang, *Environ. Geochem. Health*, 2020, **42**, 1579–1587.
3 J. Xiao, R. Hu and G. Chen, *J. Hazard. Mater.*, 2020, **387**, 121980.
4 Y. Yao, B. Gao, J. Chen and L. Yang, *Environ. Sci. Technol.*, 2013, **47**, 8700–8708.
5 M. Kumar, X. Xiong, Z. Wan, Y. Sun, D. C. Tsang, J. Gupta, B. Gao, X. Cao, J. Tang and Y. S. Ok, *Bioresour. Technol.*, 2020, **312**, 123613.
6 S. O. Amusat, T. G. Kebede, S. Dube and M. M. Nindi, *J. Water Process. Eng.*, 2021, **41**, 101993.
7 J. Huang, A. R. Zimmerman, H. Chen and B. Gao, *Environ. Pollut.*, 2020, **258**, 113809.
8 Q. Zhang, J. Wang, H. Lyu, Q. Zhao, L. Jiang and L. Liu, *Sci. Total Environ.*, 2019, **659**, 1537–1545.
9 Z. Zhuang, L. Wang and J. Tang, *J. Hazard. Mater.*, 2021, **406**, 124676.
10 N. Cheng, B. Wang, P. Wu, X. Lee, Y. Xing, M. Chen and B. Gao, *Environ. Pollut.*, 2021, **273**, 116448.
11 X. Wei, X. Wang, B. Gao, W. Zou and L. Dong, *ACS Omega*, 2020, **5**, 5748–5755.

12 Y. L. Zheng, Y. S. Wan, J. J. Chen, H. Chen and B. Gao, *Chemosphere*, 2020, 243.
13 D. Shan, S. Deng, T. Zhao, B. Wang, Y. Wang, J. Huang, G. Yu, J. Winglee and M. R. Wiesner, *J. Hazard. Mater.*, 2016, **305**, 156–163.
14 Y. F. Li, A. R. Zimmerman, F. He, J. J. Chen, L. J. Han, H. Chen, X. Hu and B. Gao, *Sci. Total Environ.*, 2020, 722.
15 X. Yang, Z. Liu, Y. Jiang, F. Li, B. Xue, Z. Dong, M. Ding, R. Chen, Q. Yang, T. An, X. Shao and L. Wang, *Appl. Clay Sci.*, 2020, 199.
16 F. Li, Y. S. Wan, J. J. Chen, X. Hu, D. C. W. Tsang, H. L. Wang and B. Gao, *Chemosphere*, 2020, 260.
17 H. Liu, L. Chang, W. Liu, Z. Xiong, Y. Zhao and J. Zhang, *Chem. Eng. J.*, 2020, **379**, 122263.
18 Z. Zhang, W. Gui, J. Wei, Y. Cui, P. Li, Z. Jia and P. Kong, *ACS Omega*, 2021, **6**, 19586–19595.
19 X. Yang, Z. Liu, Y. Jiang, F. Li, B. Xue, Z. Dong, M. Ding, R. Chen, Q. Yang and T. An, *Appl. Clay Sci.*, 2020, **199**, 105877.
20 X. Gui, C. Liu, F. Li and J. J. E. Wang, *J. Ecotoxicol. Environ. Saf.*, 2020, **197**, 110597.
21 F. Yu, F. Tian, H. Zou, Z. Ye, C. Peng, J. Huang, Y. Zheng, Y. Zhang, Y. Yang, X. Wei and B. Gao, *J. Hazard. Mater.*, 2021, **415**, 125511.
22 G. Wang, F. Liu, M. Tariq, J. Wan, W. Liang, W. Zhang, C. Peng and J. Yang, *J. Cleaner Prod.*, 2022, 343.
23 F. Li, A. R. Zimmerman, X. Hu and B. Gao, *Chemosphere*, 2020, **260**, 127610.
24 G. Quan, F. Sui, M. Wang, L. Cui, H. Wang, W. Xiang, G. Li and J. Yan, *Biochem. Eng. J.*, 2022, 179.
25 Y. Cao, W. Xiao, G. Shen, G. Ji, Y. Zhang, C. Gao and L. Han, *Bioresour. Technol.*, 2019, **273**, 70–76.
26 H. Lyu, B. Gao, F. He, A. R. Zimmerman, C. Ding, H. Huang and J. Tang, *Environ. Pollut.*, 2018, **233**, 54–63.
27 Z. Yang, J. Hou, J. Wu and L. Miao, *Ecotoxicol. Environ. Saf.*, 2021, **225**, 112750.
28 F. Li, Y. Wan, J. Chen, X. Hu, D. C. W. Tsang, H. Wang and B. Gao, *Chemosphere*, 2020, **260**, 127566.
29 P. Zhang, B. Xue, L. Jiao, X. Meng, L. Zhang, B. Li and H. Sun, *Sci. Total Environ.*, 2022, **813**, 152648.
30 Y. Zhang, Y. Zheng, Y. Yang, J. Huang, A. R. Zimmerman, H. Chen, X. Hu and B. Gao, *Bioresour. Technol.*, 2021, **337**, 125432.
31 C. Guo, J. Zou, J. Yang, K. Wang and S. Song, *PLoS One*, 2020, **15**, e0238105.
32 B. Wang, B. Gao and Y. Wan, *J. Ind. Eng. Chem.*, 2018, **61**, 161–168.
33 F. Li, X. Cao, L. Zhao, J. Wang and Z. Ding, *Environ. Sci. Technol.*, 2014, **48**, 11211–11217.
34 F. Yang, L. Zhao, B. Gao, X. Xu and X. Cao, *Environ. Sci. Technol.*, 2016, **50**, 2264–2271.
35 D. Liu, P. Yuan, D. Tan, H. Liu, T. Wang, M. Fan, J. Zhu and H. He, *J. Colloid Interface Sci.*, 2012, **388**, 176–184.
36 L. Xu, Y. Liu, J. Wang, Y. Tang and Z. Zhang, *J. Hazard. Mater.*, 2021, **404**, 124140.
37 H. Zhu and H. Zou, *Water Sci. Technol.*, 2021, **84**, 3716–3725.
38 G. Wang, F. Liu, M. Tariq, J. Wan, W. Liang, W. Zhang, C. Peng and J. Yang, *J. Cleaner Prod.*, 2022, **343**, 131085.
39 S. Cui, R. Zhang, Y. Peng, X. Gao, Z. Li, B. Fan, C. Y. Guan, J. Beiyuan, Y. Zhou, J. Liu, Q. Chen, J. Sheng and L. Guo, *J. Hazard. Mater.*, 2021, **416**, 126258.
40 Y. Peng, Y. Sun, A. Hanif, J. Shang, Z. Shen, D. Hou, Y. Zhou, Q. Chen, Y. S. Ok and D. C. W. Tsang, *J. Cleaner Prod.*, 2021, 289.
41 F. Lian, G. Cui, Z. Liu, L. Duo, G. Zhang and B. Xing, *J. Environ. Manage.*, 2016, **176**, 61–68.
42 X. Xu, Z. Xu, J. Huang, B. Gao, L. Zhao, H. Qiu and X. Cao, *Chem. Eng. J.*, 2021, 413.
43 Y. Peng, Y. Sun, B. Fan, S. Zhang, N. S. Bolan, Q. Chen and D. C. W. Tsang, *J. Cleaner Prod.*, 2021, 279.
44 G. Yin, X. Song, L. Tao, B. Sarkar, A. K. Sarmah, W. Zhang, Q. Lin, R. Xiao, Q. Liu and H. Wang, *Chem. Eng. J.*, 2020, 389.
45 S. Tayibi, F. Monlau, N. E. Fayoud, E. Abdeljaoued, H. Hannache, Y. Zeroual, A. Oukarroum and A. Barakat, *ACS Omega*, 2021, **6**, 159–171.
46 L. Chen, Z. Li, W. Li, Z. Chen, G. Chen, W. Yang, X. Zhang and X. Liu, *ACS Omega*, 2021, **6**, 16402–16409.
47 R. Gong, K. Zhong, Y. Hu, J. Chen and G. Zhu, *J. Environ. Manage.*, 2008, **88**, 875–880.
48 Y. Xiang, Z. Xu, Y. Zhou, Y. Wei, X. Long, Y. He, D. Zhi, J. Yang and L. Luo, *Chemosphere*, 2019, **237**, 124464.
49 P. Wang, L. Tang, X. Wei, G. Zeng, Y. Zhou, Y. Deng, J. Wang, Z. Xie and W. Fang, *Appl. Surf. Sci.*, 2017, **392**, 391–401.
50 X. Peng, F. Hu, T. Zhang, F. Qiu and H. Dai, *Bioresour. Technol.*, 2018, **249**, 924–934.
51 J. Guo, C. Yan, Z. Luo, H. Fang, S. Hu and Y. Cao, *J. Environ. Sci.*, 2019, **85**, 168–176.
52 G. Li, W. Zhu, C. Zhang, S. Zhang, L. Liu, L. Zhu and W. Zhao, *Bioresour. Technol.*, 2016, **206**, 16–22.
53 S. Fan, J. Tang, Y. Wang, H. Li, H. Zhang, J. Tang, Z. Wang and X. Li, *J. Mol. Liq.*, 2016, **220**, 432–441.
54 Z. Ding, Y. Wan, X. Hu, S. Wang, A. R. Zimmerman and B. Gao, *J. Ind. Eng. Chem.*, 2016, **37**, 261–267.
55 L. Sun, S. Wan and W. Luo, *Bioresour. Technol.*, 2013, **140**, 406–413.
56 W. Huang, J. Chen and J. Zhang, *Environ. Sci. Pollut. Res. Int.*, 2018, **25**, 29256–29266.
57 Y. Hu, T. Guo, X. Ye, Q. Li, M. Guo, H. Liu and Z. Wu, *Chem. Eng. J.*, 2013, **228**, 392–397.
58 P. Wang, L. Tang, X. Wei, G. Zeng, Y. Zeng, Y. Deng, J. Wang, Z. Xie and W. Fang, *Appl. Surf. Sci.*, 2017, **392**, 391–401.